Journal of Nuclear Materials 90 (1980) 193–204

MICROSTRUCTURE DEPENDENCE OF IRRADIATION CREEP AND GROWTH OF ZIRCONIUM ALLOYS

R.A. HOLT

Metallurgical Engineering Branch, Atomic Energy of Canada Limited, Chalk River Nuclear Laboratories, Chalk River, Ontario K0J 1J0, Canada

Received 1 November 1979

Zirconium alloys exhibit both irradiation creep and irradiation growth. The mechanisms governing these processes determine the sensitivity of their rates to variables such as temperature, stress, neutron flux, and microstructure. In this paper I compare the observed relationships between creep and growth of zirconium alloys and dislocation density, grain structure, and crystallographic texture with the predictions of theoretical models. The approximately linear dependence of growth on dislocation density and its dependence on texture and grain shape are consistent with a model in which there is a net flux of interstitials to edge dislocations, and vacancies arrive at grain boundaries by pipe diffusion down screw dislocations. The insensitivity of irradiation creep to dislocation density and its dependence on texture are consistent with a climb-plus-glide model in which dislocations climb out of sub-boundaries and glide across the subgrains.

1. Introduction

The effects of microstructure, i.e., grain size, grain shape, crystallographic texture and dislocation density on irradiation creep and growth of zirconium alloys are important. Microstructures varies with fabrication and chemical composition, and it is necessary to understand its effect in order to predict behaviour of different alloys fabricated in different ways. Knowledge of the relationships between microstructure and creep and growth help us to understand the controlling mechanisms.

In this paper I will compare the predictions of currently favoured models for irradiation creep and growth of zirconium alloys with available experimental data on the effects of grain shape, grain size, dislocation density and crystallographic texture. I will limit the discussion to the long term, approximately steady-state, behaviour observed under conditions pertinent to the operation of zirconium alloy components in water-cooled power reactors [1] ($\phi \leqslant 1 \times 10^{18}$ n/m^2 · s > 1 MeV, $\phi t \geqslant 1 \times 10^{25}$ n/m^2 $>$ 1 MeV, $\sigma \leqslant 150$ MPa, 530 K $\leqslant T \leqslant$ 620 K) *.

* Symbols used throughout are defined in table 1.

2. Irradiation growth

2.1. Proposed models relating irradiation growth to microstructure

2.1.1. Role of sinks for point defects

Irradiation growth of zirconium alloys is caused by the segregation to different sinks of the vacancies and interstitials generated by irradiation, but the dominant types of sinks for each type of point defect and the mode of transport of point defects to sinks are not clearly established.

Interstitials segregate to sinks with long range strain fields (biased sinks), i.e., edge dislocations and prismatic dislocation loops [2–4]. However the relative importance of prismatic loops seems to be small in terms of strain [5] and I will consider the possibility, suggested recently [6] that they are only weakly biased. Loop character (vacancy versus interstitial) has not been established at low irradiation temperatures (<620 K) and will be treated as a variable.

Vacancies segregate to sinks without long range strain fields (neutral sinks). In recent theoretical studies depleted zones [7,8], grain boundaries [2,9, 10], and subgrain boundaries [8,10,11], have been

considered as neutral sinks. We have argued [10] that the long term, steady-state irradiation growth rate in cold-worked materials, which produces a strain not recoverable on heating after irradiation [12], must result from the segregation of vacancies to grain boundaries and thus reflect the grain boundary anisotropy. MacEwen [13,14] has recently suggested the possibility that screw dislocations may act as neutral sinks. Segregation of vacancies to screw dislocations and interstitials to edge dislocations and loops would cause no net strain if the screw dislocations formed helices. However screw dislocations could be point defect pipes, allowing more rapid transport of vacancies to grain boundaries than lattice diffusion and this has a strong influence on the microstructure dependence of the growth rate.

2.1.2. Anisotropy of growth

In the absence of a preferred orientation distribution of dislocation Burgers vectors resulting from cold-work, both network dislocations and loops have orientation distributions related to crystallographic texture, and the growth strains due to segregation of interstitials to dislocations or loops and vacancies to grain boundaries are proportional to [10]

$$G_d = 1 - F_d - 2A_d\,, \tag{1}$$

$$A_d \approx \frac{1}{d_d}\left(\sum_{i=1}^{3}\frac{1}{d_d}\right)^{-1}. \tag{2}$$

2.1.3. The effect of microstructure on the rate of growth

At temperatures at which the rate of thermal vacancy formation is small compared with fast neutron effects, the sensitivity of growth rate microstructure can be calculated from [2]

$$P_i^* = (\nu_i a_i + \nu_v a_v)(C_v C_i - C_v^{th} C_i^{th}) + \sum_k P_i^k \nu_i (C_i - C_i^{th})\,, \tag{3}$$

$$P_v^* = (\nu_i a_i + \nu_v a_v)(C_v C_i - C_v^{th} C_i^{th}) + \sum_k P_v^k \nu_v (C_v - C_v^{th})\,. \tag{4}$$

The annihilation probabilities for various sinks P^k are given by [15]

$$P^{GB} = \frac{15b^2}{6(d_e/2)^2} \tag{5}$$

for grain boundaries and

$$P^D = \frac{b^2\rho}{9\left[\ln(x/r_c) - \frac{3}{4}\right]}\,, \quad x = 1/\sqrt{\rho} \tag{6}$$

for dislocations.

For screw dislocations the capture radius r_c is taken as b and for edge dislocations [16]

$$r_c = \frac{b\Omega G(1+\nu)\,\upsilon_\alpha}{3\pi kT(1-\nu)}\,. \tag{7}$$

No attempt was made to model the evolution of the loop structure. Steady values are reached after $\approx 1 \times 10^{25}$ n/m$^2 > 1$ MeV. At high temperatures ($\geqslant$670 K) at least half of the loops seem to be vacancy loops but loop character has not been assessed below 620 K [17]. The steady distribution can be treated in a number of ways:

(A) As a distribution of growing interstitial loops, disappearing by incorporation into the network at large sizes;

(B) as a distribution of vacancy loops, generated by collapse of displacement spekes, and shrinking by interstitial absorption;

(C) as a population of vacancy loops, nucleated early in the irradiation, and reaching an approximately stable size due to an increase in bias factor with loop radius [6].

For the purposes of calculating the sensitivity of growth rates to microstructural variables for cases A and B, the annihilation probability for loops, per length of dislocation line was considered equal to that for network dislocations where

$$\rho_L = N_L D_L\,. \tag{8}$$

The interstitial generation rate, P_i^*, was taken as a fraction, w, of the displacement rate, itself linearly dependent on fast flux [18]. The vacancy generation rate was taken as

$$P_v^* = P_i^*(1 - E)\,, \tag{9}$$

where EP_i^* is the rate at which vacancies at the cores of displacement spikes collapse to form new vacancy

loops *. At steady-state, the net flux of interstitials to vacancy loops must equal the rate of generation of vacancy loops.

$$EP_i^* = P_i^{VL}\nu_i(C_i - C_i^{th}) - P_v^{VL}\nu_v(C_v - C_v^{th}) . \qquad (10)$$

For biased loops (cases A and B) assumed steady values of N_L and E fix the proportion of vacancy loops according to eq. (10) (i.e., for $E = 0$, $\rho_{VL} = 0$, ρ_{VL} increases with E). For case C, no new vacancy loops are assumed to form and $E = 0$.

Fluxes of interstitials and vacancies to the various sinks were calculated for the values of physical constants, microstructural parameters and environmental parameters shown in table 2 and selected as reasonable for conditions pertinent to most of the irradiation growth data available. The rates calculated were sensitive to P_i^*, ν_v as affected by temperature and vacancy migration energy, υ_i and υ_v and insensitive to order of magnitude variations in ν_i, C_v^{th} and C_i^{th}. Other physical constants and parameters were not varied.

To simplify the description of the numerical results I will use the following terminology:
LD rate = The growth rate when vacancies are assumed to arrive at grain boundaries by lattice diffusion only. Proportional to the net arrival rate of interstitials at all dislocations and loops.
PLD rate = The growth rate when vacancies are assumed to arrive at grain boundaries by both lattice diffusion and by pipe diffusion down screw dislocations at a rapid rate. Proportional to the net arrival rate of interstitials at edge dislocations and loops.

When loops are ignored the LD rate passes through a broad maximum with increasing network dislocation density. At grain sizes, d_e, $\leqslant 3$ μm, it is relatively insensitive to network density in the range 10^{14} to 10^{15} m^{-2}, but inversely proportional to grain size to the power of 1.3 to 2.0. The PLD rate is approximately proportional to network dislocation density over the whole range, and relatively insensitive to grain size (fig. 1). The absolute value of the PLD rates calculated for grain sizes and network dislocation densities typical of cold-worked Zircaloy (6 to 30 μm, 10^{14} to 10^{15} m^{-2}) approach the observed growth rates for the flux level assumed (2.5×10^{17}

* The rate at which insterstitials nucleate loops is assumed to be negligibly small compared with EP_i^*.

Table 1
Definition of symbols

G_d	Growth anisotropy factor in d direction
F_d	Resolved fraction of basal plane normals in d direction
A_d	Grain boundary anisotropy factor in d direction
d_d, d_1, d_2, d_3	Grain sizes in the d, 1, 2, 3 directions
d_e	Effective grain size
P_i^*, P_v^*	Generation of interstitials, vacancies, by fast flux
a_i, a_v	Number of sites from which instantaneous recombination of an interstitial or vacancy can occur
ν_i, ν_v	Interstital and vacancy jump frequencies
C_i, C_v	Interstitial and vacancy concentrations
C_i^{th}, C_v^{th}	Equilibrium interstital and vacancy concentrations
P^k, P_i^k, P_v^k	Annihilation probability at the kth type of sink, for interstitials, vacancies
b	Burgers vector
$\rho, \rho_N, \rho_L, \rho_{VL}, \rho_{IL}, \rho_m$	Dislocation densities; total, network, loop, vacancy loop, interstitial loop, mobile
r_c	Capture radius of dislocation for point defects
Ω	Atomic volume
G, K, μ	Shear modulus, stiffness modulus, Poisson's ratio
υ_i, υ_v	Relaxation volume for interstitials, vacancies
k, T	Boltzman constant, temperature
ϕ	Fast flux
ϕt	$\int \phi \, dt$, integrated fast flux, t = time
σ	Applied stress
N_L, N_{IL}	Number density of loops, interstitial loops
D_L, D_{IL}	Mean loop diameter, mean interstitial loop diameter
W	Cascade efficiency, fraction of displacements giving free interstitials
E	Collapse efficiency, fraction of vacancies generated collapsing to loops
V_c	Climb velocity
l, h	Glide distance, glide height
λ	Subgrain or cell size

Table 1 (continued)

δ, η	Spacing of dislocations; in cell walls, average
$\dot{e}_{yc}, \dot{e}_{th}, \dot{e}_{CPG}, \dot{e}_g$	Strain rates; yielding creep, thermal creep, climb-plus-glide, growth
A	Constant for thermal creep
n, m	Stress exponents for thermal, irradiation creep
I	Internal stress generated by growth
s, q, f	Dislocation density exponents for growth, thermal creep, yielding creep
H	Geometric constant

$n/m^2 \cdot s > 1$ MeV), i.e., 2×10^{-11} s^{-1}. The LD rates are an order of magnitude or more lower.

The effect of a loop distribution similar to that observed in cold-worked Zircaloy after 1.6×10^{25} $n/m^2 > 1$ MeV [5] (table 2) was examined. When the loops were considered as biased interstitial loops (case A), the sensitivity of both LD and PLD rates to network dislocation density was reduced, and the sensitivity to grain size increased at low network and fine grain sizes (fig. 2). The linear sensitivity of the PLD rate to network dislocation density, and its relative insensitivity to grain size were retained for grain size $d_e \geqslant 3$ μm and network dislocation densities $\rho_N \geqslant 10^{14}$ m^{-2}.

When the loops were considered to be biased, but 30 to 80% vacancy loops ($E = 0.004$, case A + B) the sensitivity of the PLD rate to network dislocation density at low network densities and fine grain sizes was restored slightly, but there was no other effect. When the loops were considered as stable vacancy loops (case C) the only effect, compared with ignoring the loops altogether, was to reduce both rates by up to 20%.

2.2. Observations of the microstructure dependence of irradiation growth

The dependence of irradiation growth on cold-work has been clearly demonstrated [12,22]. Both increasing anisotropy due to grain elongation [9,10] and sensitivity of irradiation growth to network dis-

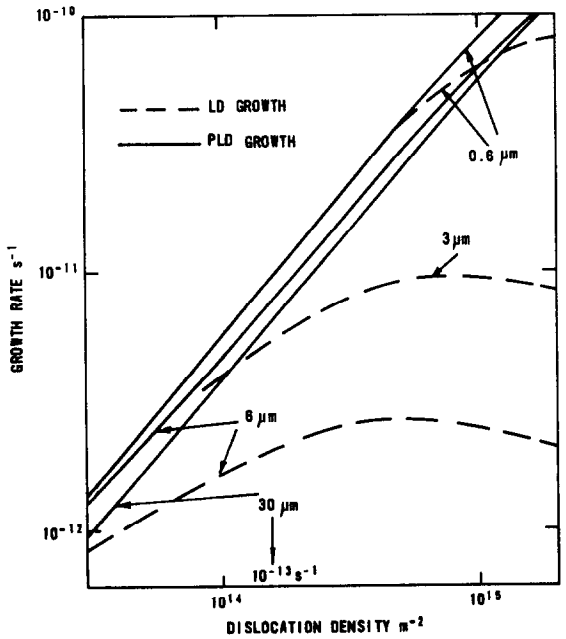

Fig. 1. Comparison of growth rates calculated for lattice diffusion of vacancies to grain boundaries (LD) and screw dislocations acting as vacancy pipes (PLD) with no loop present.

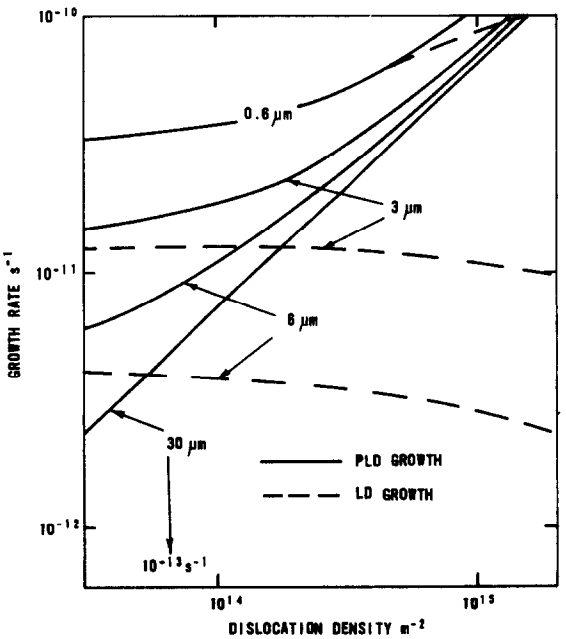

Fig. 2. Comparison of growth rates calculated for lattice diffusion to grain boundaries (LD) and screw dislocations acting as vacancy pipes (PLD) with biased interstitial loops.

Table 2
Values of parameters and constant used in calculations [a)]

(A) Physical parameters and constants	
Fast Flux, ϕ(n/m^2 · s); displacement rate (dpa/s) [18]	2.5×10^{17}; 2×10^{-8}
Cascade efficiency, W [11]	0.05, 0.10, <u>0.20</u>
Temperature, T (K)	540–575
Number of sites from which an instantaneous recombination can occur, a_i, a_v [19,20]	50
Interstitial jump frequency, ν_i, s^{-1} [19,21]	1×10^{14} exp $-Q_1/kT$, Q_1 = 0.35 eV
Vacancy jump frequency, ν_v, s^{-1} [19,21]	4×10^{14} exp $-Q_2/kT$, Q_2 = 1.3, <u>1.35</u>, 1.4 eV
Equilibrium interstitial concentration, C_I^{th} [11,19]	10 exp $-Q_3/kT$, Q_3 = 4.0 eV
Equilibrium vacancy concentration, C_V^{th} [19,21]	4 exp $-Q_4/kT$, Q_4 = 1.4 eV
Burgers vector, b (m)	3×10^{-10}
Shear modulus, G (MPa)	2.5×10^4
Atomic volume, Ω (m^3)	2.4×10^{-29}
Interstitial relaxation volume, v_i	0.27, <u>0.45</u>, 1.08
Vacancy relaxation volume, v_v	<u>−0.09</u>, −0.18
Cascade collapse efficiency, E	0.00, <u>0.004</u>, 0.007
(B) Microstructural parameters and constants	
Mean loop diameter, D_L (m) [5]	1.45×10^{-8}
Mean loop density, N_L (m^{-3}) [5]	$\underline{5}–10 \times 10^{21}$
Network dislocation density, ρ_N (m^{-2})	$\underline{10^{13}}–10^{16}$
Effective grain size, d (m)	$0.6–30 \times 10^{-6}$
Ratio of screw to edge dislocation densities	1.0

[a)] Values underlined are those used in numerical examples shown unless otherwise specified.

location density could account for increasing growth rates with increasing cold-work. No experiment has been carried out in which grain shape and dislocation density have been varied independently and a long term growth rate established.

The observation that material with 25% cold-work and relatively equiaxed grains demonstrates a much higher growth rate than annealed material [22, 23] suggests sensitivity to network density. The elongation and diametral strain rate of pressure tubes manufactured by eight different routes were analysed to separate growth and creep, assuming the grain shape and texture dependence given by eq. (1) [24]. The growth rates thus establish agreed well with data for small unstresses specimens, suggesting that the treatment was valid. The growth rates of the pressure tubes varied with $\rho_N^{0.82}$ (fig. 3).

To try to substantiate this relationship, the grain

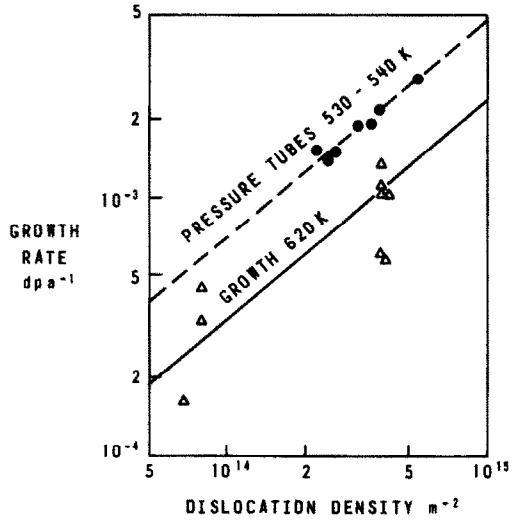

Fig. 3. Effect of dislocation density on irradiation growth rate of cold worked Zircaloy.

Table 3
Microstructural observations on Zircaloy strip irradiated by Adamson [13]

Condition	Texture, F_d		Dislocation density (m^{-2})	Grain size (μm)		
	Transverse	Longitudinal		Thickness	Transverse	Longitudinal
20% cold-work, stress-relieved at 780 K	0.17	0.10	0.8×10^{14}	8.2	16.4	14.1
40% cold-work, stress-relieved at 780 K	0.17	0.17	0.7×10^{14}	8.2	19.0	18.3
60% cold-work, stress-relieved at 710 K	0.12	0.14	3.7×10^{14}	7.8	22.5	17.5
80% cold-work, stress-relieved at 710 K	0.17	0.14	3.8×10^{14}	6.5	22.0	22.9

structures and dislocation densities of material irradiated by Adamson [12] at 620 K were measured by techniques used previously [24] (table 3). The long term growth rates of both transverse and longitudinal specimens at doses of 1.6 to 2.0×10^{25} ($n/m^2 > 1$ MeV) were estimated by subtracting the growth strains of annealed materials irradiated to the same dose, and assuming linear dose dependence. The growth rates of 20 and 40% cold-worked materials, stress relieved at 780 K, were much lower than those of 60 and 80% cold-worked material stress relieved at 710 K, in spite of similar grain boundary anisotropy. After correction for grain boundary anisotropy and texture the results suggest a dependence of growth rate on dislocation density similar to that derived from pressure tube behaviour (fig. 3).

The only information relating grain size to irradiation growth rate is that for the pressure tubes operating in power reactors [24]. Tubes with similar dislocation densities and a factor of two variation in grain size had similar growth rates (table 4).

3. Irradiation creep

3.1. Models for microstructure dependence of irradiation creep

The mechanisms of irradiation creep are still in question. The SIPA mechanism (Stress Induced Preferential Absorption) is currently favoured to explain irradiation creep in fast reactor steels [16,25,26] and has been considered for zirconium alloys [27]. The climb-plus-glide mechanism [28], in which the climb caused by the preferential absorption of interstitials at edge dislocations allows them to glide, is currently favoured for zirconium alloys [29,30] and under some conditions may contribute substantial strain in steels [31]. For this mechanism the obstacles to glide have not been established. The yielding creep mechanism [32] agrees with sime aspects of irradiation creep behaviour of cold-worked Zircaloy. It has been criticized on the basis of single crystal and transient behaviour [28,29] but cannot be

Table 4
Effect of grain size on growth rate of pressure tubes [21]

Tube type	Growth rate [a] ($m^2/n > 1$ MeV)	Dislocation density (m^{-2})	Effective grain size (μm)
Hanford 1a 17.5% cold-work	1.8×10^{-28}	2.2×10^{14}	18.5
Hanford 3 17.5% cold-work	1.8×10^{-28}	2.6×10^{14}	15.3
Winfrith A 30% cold-work	1.7×10^{-28}	2.5×10^{14}	10.1

[a] Corrected for grain shape and texture.

ruled out as a dominant long-term mechanism in cold-worked material.

3.1.1. SIPA model

The rate of SIPA creep can be calculated using eqs. (3) to (7), if the expression for the capture radius of a dislocation is modified to take into account the modulus interaction between dislocations and point defects [16]

$$r_c = \frac{Gb\Omega}{\pi kT}\left[\left(\frac{1+\nu}{1-\nu}\right)\frac{v_\alpha}{3} + A_\alpha^\beta \frac{\sigma}{G}\right] . \qquad (7a)$$

Here, A_α^β is a function of the differences, ΔG_α, ΔK_α, in shear modulus, G, and stiffness modulus, K, between the matrix and a vacancy or interstitial (designated by α = v or α = i). The full expressions are given by Heald and Speight [16].

The SIPA creep rate is the stress induced increase in the net flux of interstitials to edge dislocations with Burgers vectors parallel to applied stress. For extreme values of the modulus differences ($\Delta G_i = -G$, $\Delta G_v = -G$, $\Delta K_i = K$, $\Delta K_v = -K$) the magnitudes of the calculated SIPA creep rates only approach those of the growth rate for stresses of several hundred MPa. Similar creep and growth rates are observed experimentally at stresses around 100 MPa [24].

The SIPA creep rates are insensitive to grain size. If no loops or only stable vacancy loops are present, the rate is proportional to network dislocation density to the power of 1.2 (fig. 4). If biased loops are present, the rate is insensitive to network density at low densities, and proportional to network density to a power of 0.8 at high densities (fig. 4). The insensitivity of the SIPA rate to initial dislocation density claimed by Bullough and Hayns [24] is due to their assumed dominance of the irradiation-generated dislocation structure.

The anisotropy associated with SIPA creep depends on the anisotropic orientation of dislocation Burgers vectors and has been calculated from crystallographic texture assuming that $1/3\langle 11\bar{2}0\rangle$ is the only prevalent Burgers vector [10]. For a typical tube or plate texture, the anisotropy can be expressed as the ratio of the calculated creep rate in the working direction to that in the transverse (or tangential) direction in uniaxial tests. Values of this ratio, calculated for SIPA for cold-worked Zr–2.5wt%Nb and Zircaloy pressure tubes, are given in table 5.

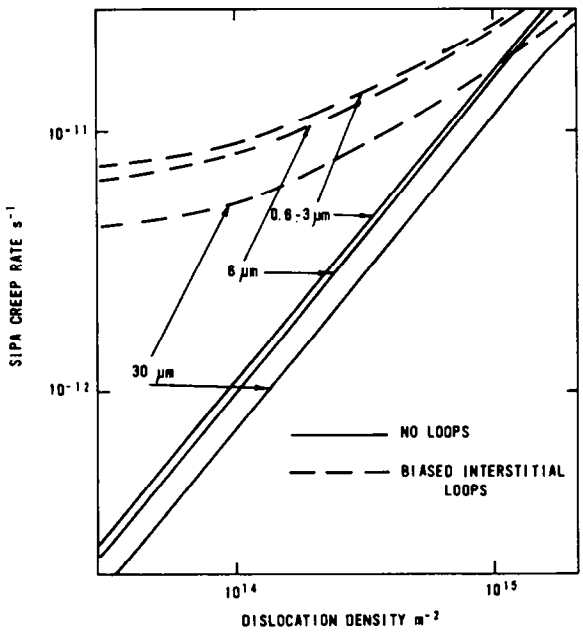

Fig. 4. Comparison of calculated SIPA creep rates with and without biased interstitial loops.

3.1.2. Climb-plus-glide model (CPG)

The creep rate resulting from the CPG mechanism is related to the climb velocity, V_c, by

$$\dot{\epsilon}_{CPG} = \rho_m V_c d/h . \qquad (11)$$

The climb velocity is given by the growth calcula-

Table 5
Anisotropy ratios (ratio of longitudinal to transverse creep rate with uniaxial stress) calculated from texture or measured

Mechanism	Anisotropy ratio	
	Cold-worked Zircaloy	Cold-worked Zr–2.5wt%Nb
SIPA	2.3	2.5
Prism slip	2.3	2.5
Basal slip	0.4	0.4
80% prism slip, 20% basal slip	1.8	1.9
Measured [a]	1.2–2.1	1.7–2.0

[a] In bent-beam stress relaxation tests.

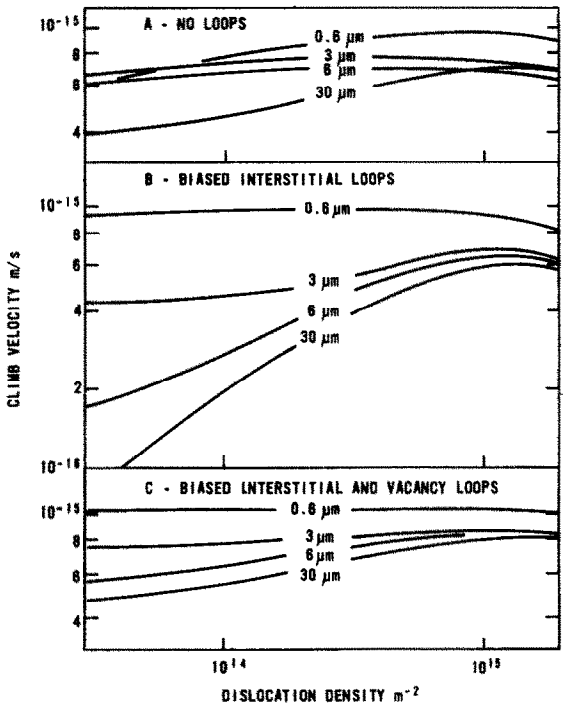

Fig. 5. Effect of microstructure on calculated climb velocity of edge dislocations in network.

tion (eqs. (3) and (4)), the stress dependence arising from the stress dependence of ρ_m. The climb velocity is relatively insensitive to network dislocation density or grain size if no loops are present (fig. 5A), or if only stable vacancy loops are considered. If only biased interstitial loops are considered, the climb velocity depends on network dislocation density and grain size only at low network densities and large grain sizes (fig. 5B). The insensitivity to microstructure is restored if 30 to 80% of the biased loops are vacancy loops (fig. 5C). Thus the sensitivity of CPG creep rate to microstructure depends predominantly on the relationship of ρ_m, l and h to network dislocation density. This depends on the nature of the rate limiting obstacles to slip.

If the obstacles are depleted zones or the loops visible in the electron microscope, then l/h is the zone or loop spacing divided by the zone or loop diameter. For the loops, this is relatively insensitive to network dislocation density. The loops observed in annealed material are smaller (6.5 versus 14.5 μm) but more numerous (2.0 versus 0.5×10^{22} m^{-3}) than in cold-worked material [5] (i.e., l/h = 6.5 versus 4.6). Thus the sensitivity of creep rate to network density is closely related to the sensitivity of mobile dislocation density to total density (probably linear). The same would probably hold for depleted zones acting as the rate controlling obstacles.

According to Gittus' *I*-Creep mechanism [33], after climbing a distance equal to the mean link length, the whole dislocation network is assumed to advance by an amount equal to the mean distance bowed out by the links in the network. Thus,

$$h = l_N = \sqrt{(3/\rho_N)} \,. \tag{12}$$

The distance bowed out can be shown to be proportional to $l_N^2(\sigma/G)$ or $\sigma/\rho_N G$ and thus the *I*-Creep rate is proportional to $\sqrt{\rho_N}$.

The dislocations in cold-worked and stress relieved and extruded zirconium alloys are arranged, more or less loosely, into cell structures [34]. If the cell walls act as rate limiting barriers to glide, then dislocations released from the cell walls by climb will glide a distance equal to the subgrain size, λ. If dislocations are released after climbing a distance proportional to the mean spacing in the wall, δ, and most of the dislocations are in the subgrain walls

$$\delta = 3/\rho_N\lambda \,, \tag{13}$$

$$\dot{\epsilon}_{CPG} \propto \frac{\rho_N V_c \lambda}{1/\rho_N\lambda} = \rho_N^2\lambda^2 V_c \,. \tag{14}$$

Observations of dislocation structures in zirconium alloys by X-ray line broadening [24,34] have shown that the coherent diffracting domain size, which appears to be related to δ is relatively insensitive to dislocation density and thus λ is inversely proportional to ρ_N. The X-ray observations are supported by thin film measurements of the subgrain size (fig. 6). In this case the CPG creep rate depends only on V_c.

The anisotropy of glide has been calculated from crystallographic texture assuming that the only Burgers vectors present are $1/3\langle 11\bar{2}0\rangle$ [7]. Values of the anisotropy ratio for slip of dislocations on $(10\bar{1}0)$, the only common slip plane, (0002) the most likely cross slip plane, and a probable combination are given in table 5.

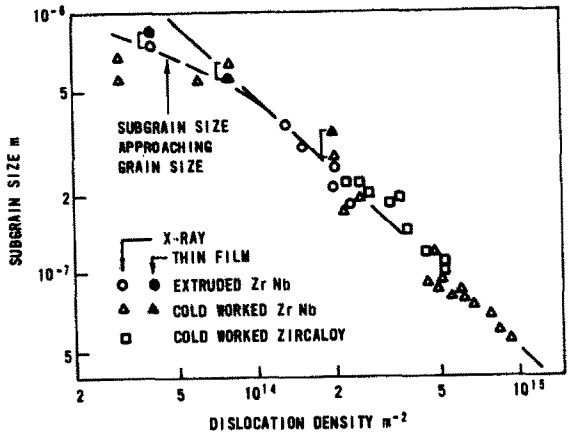

Fig. 6. Relationship between dislocation density and subgrain size in zirconium alloys.

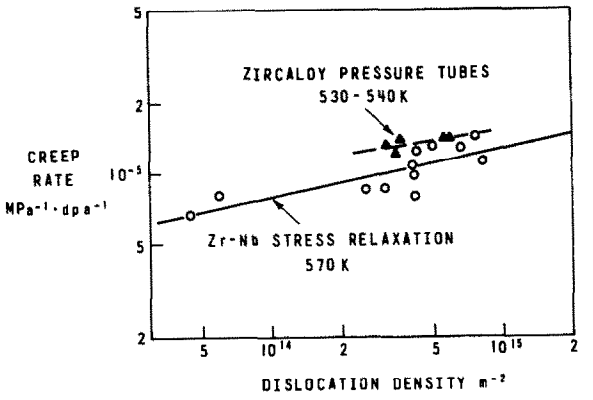

Fig. 7. Effect of dislocation density on irradiation creep rate of zirconium alloys.

3.1.3. Yielding creep model

The yielding creep rate is described by the following equations [32]

$$\dot{\epsilon}_{yc} = f\dot{\epsilon}_{th} \approx B\sigma_m \,, \tag{15a}$$

$$\dot{\epsilon}_{th} = A\sigma^n \,, \tag{15b}$$

$$f \propto (I/\sigma)^{n-m} \,, \tag{15c}$$

$$I = \left(\frac{2}{3}\right)^{1/2}\left(\frac{2\dot{\epsilon}_g}{A\sqrt{3}}\right)^{1/n} . \tag{15d}$$

Thus if

$$\dot{\epsilon}_g \propto \rho_N^s \,, \tag{16a}$$

$$A \propto \rho_N^q \,, \tag{16b}$$

$$\dot{\epsilon}_{yc} \propto \rho_N^f \,, \tag{16c}$$

then

$$f = q + (s/n)(n - m) \,. \tag{16d}$$

From section 2.2, $s = 0.8$. In the range of temperature, stress and flux of interest, $m = 1$ and $n = 3$ [35,36]. The sensitivity of the thermal creep rate to dislocation density, q, is negative for Zircaloy at short times, but at longer times appears to approach zero [35]. For Zr–2.5wt%Nb it appears to be positive [36]. Thus $f \geqslant 0.5$ depending on the value of q.

The anisotropy associated with yielding creep has not been calculated. Slip is thought to be the strain mechanism for thermal creep at 550 to 600 K. The anisotropy calculated for slip from texture depends on the stress sensitivity and it is not clear whether the anisotropy of yielding creep is that associated with the stress sensitivity of thermal creep ($n = 3$), or irradiation creep ($m = 1$).

3.2. Experimental observations of microstructure dependence of irradiation creep

Pure irradiation creep, unaffected by contributions from irradiation growth, can only be measured in bending, or by subtracting irradiation growth from total strain. Bent-beam stress relaxation tests have been used to evaluate the anisotropy of irradiation creep of zirconium alloys [37–39]. Measured creep anisotropy ratios for cold-worked Zircaloy and Zr–2.5wt%Nb are given in table 5. These are lower than the values calculated for pure prism slip and SIPA, and agree well with those for prism slip plus basal slip. When the latter model was used to evaluate the creep anisotropy of Zircaloy pressure tubes in conjunction with the growth anisotropy model expressed by eq. (1), the creep rates deduced agreed with bent-beam stress relaxation data [24]. The creep rates of the pressure tubes were insensitive to dislocation density over a fairly narrow range (fig. 7).

The in-reactor creep rates of cold-worked and stress-relieved and of extruded Zr–2.5wt%Nb alloy have been measured using bent-beam stress relaxation tests [38,39]. The dislocation densities were measured using the X-ray line broadening technique

[34] The results show that the creep rate of this alloy is also relatively insensitive to dislocation density (fig. 7). The irradiation creep rates of zirconium alloys have previously been shown to be insensitive to grain size over a wide range of grain sizes [40].

4. Discussion

The experimental data on irradiation growth agree with the model in which screw dislocations are neutral sinks and serve as vacancy pipes allowing rapid transport of vacancies to the grain boundaries. This model explains the high sensitivity of growth rate to dislocation density, its insensitivity to grain size, and gives absolute rates comparable to those observed.

The experimentally observed creep anisotropy of cold-worked and stress-relieved zirconium alloys is consistent with the climb-plus-glide model since cross slip allows the anisotropy ratio calculated for this model to be compatible with that observed. The anisotropy ratio calculated for SIPA creep is higher than that observed.

The observed insensitivity of irradiation creep to network dislocation density agrees with a climb-plus-glide model in which dislocations, released from the cell walls by climb, glide a distance equal to the cell size.

The SIPA model predicts that creep rates are sensitive to dislocation density. A high density of strongly biased interstitial loops would eliminate this sensitivity, but this is inconsistent with available information on loop character [17] and recent ideas on the interaction between point defects and loops [6]. Given the observed, almost linear sensitivity of irradiation growth to dislocation density, yielding creep rates would be sensitive to at least the square root of dislocation density. Thus both these models are inconsistent with the experimental evidence.

To fully substantiate these conclusions, good experimental data are required, particularly for irradiation growth, for which the microstructural variables have been changed independently. In most experiments fabriaction variables (e.g., cold-work) rather than microstructural variables have been used. There has, as yet, been no pure irradiation growth experiment allowing the relative roles of texture and grain shape given by eq. (1) to be tested. Confirmation of this model relies on pressure tube data for which creep is also present.

The calculated sensitivities of growth and SIPA creep rates to microstructural variables appear to relate strongly to the measureable geometry of the microstructure (e.g., the relationship between mean dislocation spacing and mean grain size) and less strongly to the less well defined physical parameters (e.g., vacancy mobility, cascade efficiency). Thus the experimental study of microstructural dependence of creep and growth complements the study of variables with effects more sensitive to physical parameters (e.g., temperature and fast neutron flux).

5. Implications

A major implication of the mechanisms discussed above is that irradiation creep and growth of zirconium alloys can be controlled by control of the microstructure. This is particularly true if loops play an insignificant role as biased sinks. Then the rate of irradiation growth can be controlled by adjusting the initial dislocation density. Tubes with very low diametral or axial strain rates can be designed by adjusting grain shape and texture. Cold-worked Zircaloy pressure tubes actually exhibit these extremes of behaviour [24].

The role of dislocation loops as biased sinks is very important. Dislocations will disappear when they climb a distance approximately equal to the mean spacing, $\eta \propto 1/\sqrt{\rho_N}$, and meet dislocations of opposite sign. The recovery rate is thus

$$\partial\rho_N/\partial t = -\rho_N V_c/\eta = -H\rho_N^{3/2} V_c \,. \tag{17a}$$

If the loops are strongly biased sinks [4] the dislocation network will be regenerated by the growth of interstitial loops. With an interstitial loop density, N_{IL}, and mean diameter, D_{IL}, edge dislocation length is generated at a rate

$$\partial\rho/\partial t = \pi N_{IL}\, \mathrm{d}D_{IL}/\mathrm{d}t \,. \tag{17b}$$

At steady-state, the dislocation density in loops remain constant so eq. (17b) gives the rate at which edge dislocations are added to the network. In the

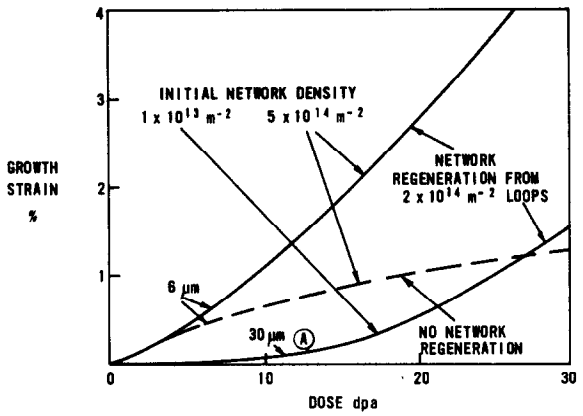

Fig. 8. Estimated effect of network dislocation regeneration resulting from loop bias model on time dependance of irradiation growth. "Breakaway" at A in initially annealed material is due to increasing pipe diffusion through network.

simple model used earlier $dD_{IL}/dt = 2V_c$ and thus the total change in network density is

$$\frac{\partial \rho_N}{\partial t} = (2\pi N_{IL} - H\rho_N^{3/2})\, V_c\,. \qquad (17c)$$

Thus the network density and growth rate tend towards steady-state values depending on grain size. Fig. 8 shows examples for two initial grain sizes and dislocation densities if H is relatively small (i.e., 0.1).

If loop bias increases with radius [6] and loop populations are stable, no regeneration occurs and both network density and growth rate decrease continuously (fig. 8).

Sufficient high dose growth data and microstructural observations are not available to distinguish definitively between the two types of behaviour, but current observations seem to support a decreasing network density [5].

6. Conclusions

Currently available data relating irradiation creep and growth of zirconium alloys to microstructure, under conditions of interest for the operation of pressure tubes and fuel sheating in water-cooled power reactors, suggest that:

– Growth results from a net flux of interstitials to edge dislocations and prismatic loops and a net flux of vacancies arrives at grain boundaries by pipe diffusion down screw dislocations.

– Irradiation creep is consistent with the climb-plus-glide model, in which the glide is blocked by the cell walls of the network dislocation structure.

In order to confirm these models, better experimental data are required, in particular, examining the anisotropy and dislocation density dependence of growth.

Acknowledgements

I would like to thank G.J.C. Carpenter, V. Fidleris and S.R. MacEwen for helpful discussions, A.R. Causey for permission to quote unpublished results, R.B. Adamson for providing specimens of materials for which growth data were available, and D. Hartwig and J.E. Winegar for technical assistance.

References

[1] V. Fidleris, At. Energy Rev. 13 (1975) 51.
[2] H. Wiedersich, Physical Metallurgy of Reactor Fuel Elements (The Metals Society, London, 1973) p. 142.
[3] W.G. Wolfer and M. Ashkin, J. Appl. Phys. 47 (1976) 791.
[4] W.G. Wolfer and M. Ashkin, J. Appl. Phys. 46 (1975) 547.
[5] G.J.C. Carpenter and D.O. Northwood, J. Nucl. Mater. 56 (1975) 260.
[6] R. Bullough, M.R. Hayns and C.H. Woo, AERE, Harwell Report TP 733 (1979).
[7] F.A. Nichols, J. Nucl. Mater. 30 (1969) 249.
[8] C.C. Dollins, J. Nucl. Mater. 59 (1976) 61.
[9] D. Fainstein–Pedraza, E.J. Savino and H.J. Pedraza, J. Nucl. Mater. 73 (1978) 151.
[10] R.A. Holt and E.F. Ibrahim, Acta Met. 27 (1979) 1319.
[11] S.R. MacEwen, J. Nucl. Mater. 54 (1974) 85.
[12] R.B. Adamson, ASTM STP 633 (1977) p. 326.
[13] S.R. MacEwen, private communication.
[14] S.R. MacEwen and G.J.C. Carpenter, J. Nucl. Mater. 90 (1980) 111.
[15] S.R. MacEwen and I.J. Hastings, Phil. Mag. 31 (1975) 135.
[16] P.T. Heals and M.V. Speight, Acta Met. 23 (1975) 1389.
[17] D.O. Northwood, R.W. Gilbert, L.E. Bahen, P.M. Kelly, R.G. Blake, A. Jostsons, P.K. Madden, D. Faulkner, W. Bell and R.B. Adamson, J. Nucl. Mater. 79 (1979) 379.

[18] C.H. Woo, Atomic Energy of Canada Limited, Report AECL-6189 (1978).
[19] A.C. Damask and G.J. Diennes, Point Defects in Metals (Gordon and Breach, New York, 1971).
[20] P. Vialaret, F. Moreau, A. Bessis, C. Dimitrov and O. Dimitrov, J. Nucl. Mater. 55 (1978) 83.
[21] G.M. Hood, Atomic Energy of Canada Limited, Report AECL-5672 (1977).
[22] R.A. Murgatroyd and A. Rogerson, Paper presented at 4th ASTM Intern. Conf. on Zirconium in the Nuclear Industry, Stratford-on-Avon, 1978.
[23] R.A. Murgatroyd and A. Rogerson, J. Nucl. Mater. 79 (1979) 302.
[24] R.A. Holt, J. Nucl. Mater., to be published.
[25] R. Bullough and M.R. Hayns, J. Nucl. Mater. 65 (1977) 184.
[26] W.G. Wolfer, J. Nucl. Mater. 90 (1980) 175.
[27] C.H. Woo, J. Nucl. Mater. 80 (1979) 132.
[28] G.R. Piercy, J. Nucl. Mater. 26 (1968) 18.
[29] S.R. MacEwen and V. Fidleris, Phil. Mag. 31 (1975) 1149.
[30] S.R. MacEwen and V. Fidleris, J. Nucl. Mater. 65 (1977) 250.
[31] P.T. Heald and J.E. Harbottle, J. Nucl. Mater. 67 (1977) 229.
[32] P.K. Madden and R. Hesketh, CEGB, Report RD/B/N3113 (1975).
[33] J. Gittus, Phil. Mag. 25 (1972) 345.
[34] R.A. Holt, J. Nucl. Mater. 59 (1976) 234.
[35] E.F. Ibrahim, J. Nucl. Mater. 46 (1973) 169.
[36] E.F. Ibrahim, ASTM STP 551 (1974) p. 249.
[37] A.R. Causey, J. Nucl. Mater. 54 (1974) 64.
[38] C.E. Coleman, A.R. Causey and V. Fidleris, Atomic Energy of Canada Limited, Report AECL-5042 (1975).
[39] A.R. Causey, unpublished data.
[40] A.R. Causey, ASTM STP 551 (1974) p. 263.